

Tentative detection of the rotation of Eris

Henry G. Roe^{a,*}, Rosemary E. Pike^b, Michael E. Brown^c

^a Lowell Observatory, Flagstaff, AZ 86001, USA

^b Gemini Observatory, Hilo, HI 96720, USA

^c California Institute of Technology, Division of Geological and Planetary Sciences, Pasadena, CA 91125, USA

ARTICLE INFO

Article history:

Received 30 April 2008

Revised 28 July 2008

Available online 4 September 2008

Keywords:

Kuiper belt

ABSTRACT

We report a multi-week sequence of *B*-band photometric measurements of the dwarf planet Eris using the *Swift* satellite. The use of an observatory in low-Earth orbit provides better temporal sampling than is available with a ground-based telescope. We find no compelling evidence for an unusually slow rotation period of multiple days, as has been suggested previously. A ~ 1.08 day rotation period is marginally detected at a modest level of statistical confidence ($\sim 97\%$). Analysis of the combination of the *Swift* data with the ground-based *B*-band measurements of Rabinowitz et al. [Rabinowitz, D.L., Schaefer, B.E., Tourtellotte, S.W., 2007. *Astron. J.* 133, 26–43] returns the same period (~ 1.08 day) at a slightly higher statistical confidence ($\sim 99\%$).

© 2008 Elsevier Inc. All rights reserved.

1. Introduction

The recently discovered Kuiper belt object Eris is $1.28 \pm 0.02\%$ the mass of Pluto (Brown and Schaller, 2007). The near-infrared spectrum of Eris is dominated by methane (Brown et al., 2005), suggesting that its surface, like Pluto, is covered in significant deposits of methane frost. The surface of Pluto is variegated, with regions of low and high albedo (Cruikshank et al., 1997). The heterogeneity of Pluto's surface is revealed in its light curve, which has a large amplitude of 0.33 magnitude (Buie et al., 1997). The *V*-band geometric albedo of Eris ($85 \pm 7\%$; Brown et al., 2006) is approximately equal to the albedo of the brightest patches on Pluto's surface (Stern et al., 1997). This led to the suggestion that the surface of Eris is likely homogeneous and of a composition similar to the brightest patches of Pluto (Brown et al., 2006).

Pluto's rotation period (6.4 days) is set by tidal interactions with its large moon Charon. Dysnomia, the one known moon of Eris, is far too small to have significantly altered the rotation rate of Eris. Several previous observers have not conclusively identified the rotation period of Eris (Carraro et al., 2006; Lin et al., 2007; Sheppard, 2007; Rabinowitz et al., 2007; Duffard et al., 2008). The goal of the observations reported here was to measure the rotation period of Eris.

2. Observations

In December 2006 and January 2007 we acquired a sequence of images with the Ultraviolet/Optical Telescope (UVOT) of the

Swift spacecraft. The *Swift* mission was designed to detect Gamma Ray Bursts (GRB) and rapidly slew to measure their optical afterglow. Accepting the risk that observations may be interrupted to follow an evolving GRB, UVOT is available for non-GRB science. While UVOT is small (30 cm) compared with many groundbased telescopes, UVOT has two distinct advantages for this work. Being space-based UVOT is not subject to the vagaries of weather or atmospheric transparency and is therefore photometrically much more stable than a ground-based telescope. Additionally, being in low-Earth orbit UVOT can observe throughout each 24 h day, losing only ~ 45 min out of every ~ 90 min orbit, while a ground-based telescope is limited by its site to observing Eris for 6–10 h per day. These are particularly useful advantages when an object has a slow rotation period of one day or longer, such as has been suggested for Eris. Over several weeks we acquired nearly 200 ks of exposure time on Eris with UVOT in the *B* filter. Most of these images were acquired in a 2×2 binning mode with a pixel size of $1''0$. The first three images of Table 1 were acquired with no binning ($0''5/\text{pixel}$) and were rebinned to 2×2 for the analysis.

Following the photometric prescription of Li et al. (2006) we measured the magnitude of Eris in each individual frame. We found 220 frames taken between 19 December 2006 and 16 January 2007 were of usable quality. (See Table 1 for a full listing of the observations.) To refine the precision of the frame-to-frame relative photometry we also measured an ensemble of 26 comparison stars, chosen to be between 1 magnitude fainter and 2 magnitudes brighter than Eris and to appear in a minimum of 180 of the 220 frames. Several other stars that met these criteria were eliminated for having obvious photometric periodicities or trends. None of these eliminated stars displayed periodicities near the ~ 1.1 day period we find for Eris. The mean full-width at

* Corresponding author.

E-mail address: hroe@lowell.edu (H.G. Roe).

Table 1
Swift measurements.

Julian date	Exp. time (s)	B magnitude	Phase angle	Julian date	Exp. time (s)	B magnitude	Phase angle
2454088.576	390.5	19.40 ± 0.09	0°535	2454101.237	693.5	19.43 ± 0.07	0°572
2454088.643	390.5	19.37 ± 0.09	0°536	2454101.304	634.7	19.46 ± 0.08	0°572
2454088.710	391.0	19.46 ± 0.09	0°536	2454101.371	693.1	19.65 ± 0.08	0°572
2454093.585	450.4	19.53 ± 0.10	0°553	2454101.438	693.1	19.43 ± 0.07	0°572
2454093.652	450.9	19.18 ± 0.08	0°553	2454101.772	634.2	19.57 ± 0.08	0°573
2454093.719	450.8	19.43 ± 0.09	0°553	2454101.840	693.5	19.68 ± 0.08	0°573
2454093.786	450.9	19.51 ± 0.10	0°553	2454101.906	693.7	19.69 ± 0.08	0°573
2454093.853	450.5	19.28 ± 0.08	0°554	2454101.973	693.2	19.42 ± 0.07	0°573
2454093.920	450.4	19.56 ± 0.10	0°554	2454102.040	693.5	19.62 ± 0.08	0°573
2454093.987	450.9	19.67 ± 0.11	0°554	2454102.107	693.7	19.85 ± 0.10	0°573
2454094.054	451.0	19.46 ± 0.10	0°554	2454102.174	693.0	19.54 ± 0.08	0°573
2454094.121	451.0	19.40 ± 0.09	0°554	2454102.241	693.2	19.54 ± 0.08	0°573
2454094.188	451.0	19.26 ± 0.08	0°555	2454102.308	693.4	19.46 ± 0.07	0°574
2454094.255	451.5	19.53 ± 0.10	0°555	2454102.375	693.6	19.53 ± 0.07	0°574
2454094.322	450.8	19.48 ± 0.10	0°555	2454102.442	693.5	19.45 ± 0.07	0°574
2454094.389	450.9	19.62 ± 0.10	0°555	2454102.777	575.2	19.73 ± 0.10	0°574
2454094.456	450.4	19.73 ± 0.11	0°555	2454102.844	634.1	19.59 ± 0.08	0°574
2454094.522	450.9	19.37 ± 0.09	0°556	2454102.911	574.6	19.33 ± 0.07	0°574
2454094.590	451.0	19.34 ± 0.09	0°556	2454102.978	634.2	19.49 ± 0.08	0°575
2454094.656	450.9	19.44 ± 0.09	0°556	2454103.246	575.2	19.60 ± 0.09	0°575
2454094.724	450.9	19.41 ± 0.09	0°556	2454103.313	634.2	19.59 ± 0.09	0°575
2454094.790	450.4	19.59 ± 0.10	0°557	2454103.380	634.2	19.48 ± 0.08	0°575
2454094.857	450.4	19.37 ± 0.09	0°557	2454103.571	664.4	19.47 ± 0.07	0°575
2454094.924	450.4	19.35 ± 0.09	0°557	2454103.639	900.2	19.48 ± 0.06	0°576
2454094.991	449.9	19.60 ± 0.11	0°557	2454103.708	1195.2	19.40 ± 0.05	0°576
2454095.058	449.4	19.60 ± 0.10	0°557	2454103.776	1431.9	19.49 ± 0.05	0°576
2454095.125	450.8	19.48 ± 0.09	0°557	2454103.842	1196.2	19.32 ± 0.05	0°576
2454095.192	450.9	19.36 ± 0.09	0°558	2454103.909	1254.8	19.47 ± 0.06	0°576
2454095.259	450.4	19.48 ± 0.10	0°558	2454105.121	403.3	19.46 ± 0.09	0°577
2454095.326	450.5	19.34 ± 0.09	0°558	2454105.188	439.0	19.45 ± 0.09	0°578
2454095.393	450.5	19.33 ± 0.09	0°558	2454105.255	416.2	19.37 ± 0.09	0°578
2454095.460	450.5	19.86 ± 0.13	0°558	2454105.322	452.0	19.47 ± 0.09	0°578
2454095.527	450.4	19.20 ± 0.08	0°559	2454105.389	428.7	19.46 ± 0.09	0°578
2454095.597	922.9	19.52 ± 0.07	0°559	2454106.582	545.9	19.52 ± 0.08	0°579
2454095.664	863.9	19.50 ± 0.07	0°559	2454106.648	486.1	19.33 ± 0.08	0°579
2454095.731	921.9	19.50 ± 0.07	0°559	2454106.715	486.6	19.47 ± 0.09	0°579
2454095.797	923.4	19.33 ± 0.06	0°559	2454106.782	487.5	19.47 ± 0.08	0°579
2454095.862	449.0	19.32 ± 0.08	0°559	2454106.849	487.1	19.41 ± 0.08	0°579
2454095.929	450.0	19.42 ± 0.09	0°560	2454106.916	487.1	19.46 ± 0.08	0°579
2454095.996	450.1	19.57 ± 0.10	0°560	2454106.983	487.1	19.46 ± 0.09	0°579
2454096.063	450.5	19.43 ± 0.09	0°560	2454107.049	486.5	19.59 ± 0.09	0°579
2454096.129	450.5	19.31 ± 0.08	0°560	2454107.117	487.0	19.32 ± 0.08	0°580
2454096.197	450.5	19.42 ± 0.09	0°560	2454107.183	487.0	19.53 ± 0.09	0°580
2454096.263	451.0	19.24 ± 0.08	0°561	2454107.251	486.5	19.53 ± 0.09	0°580
2454096.331	450.5	19.51 ± 0.10	0°561	2454107.317	486.7	19.50 ± 0.09	0°580
2454096.397	450.4	19.51 ± 0.10	0°561	2454107.585	487.1	19.45 ± 0.08	0°580
2454096.546	1337.1	19.52 ± 0.06	0°561	2454107.652	487.2	19.39 ± 0.08	0°580
2454096.611	982.2	19.51 ± 0.06	0°561	2454107.719	487.1	19.53 ± 0.09	0°580
2454096.679	1159.4	19.39 ± 0.05	0°562	2454107.786	487.1	19.42 ± 0.08	0°580
2454096.747	1336.2	19.41 ± 0.05	0°562	2454107.853	487.2	19.39 ± 0.08	0°580
2454096.814	1336.2	19.45 ± 0.05	0°562	2454107.919	487.2	19.38 ± 0.08	0°580
2454096.881	1336.6	19.40 ± 0.05	0°562	2454107.987	487.0	19.39 ± 0.08	0°580
2454099.224	1311.0	19.39 ± 0.05	0°568	2454108.053	487.0	19.41 ± 0.08	0°580
2454099.291	1370.8	19.53 ± 0.06	0°568	2454108.121	487.7	19.44 ± 0.09	0°580
2454099.358	1312.3	19.48 ± 0.05	0°568	2454108.187	487.1	19.47 ± 0.08	0°580
2454099.425	1371.5	19.51 ± 0.05	0°568	2454108.254	487.6	19.72 ± 0.10	0°580
2454099.492	1372.5	19.40 ± 0.05	0°568	2454108.522	487.0	19.51 ± 0.09	0°580
2454099.764	574.3	19.65 ± 0.09	0°569	2454108.589	486.6	19.47 ± 0.09	0°581
2454099.831	632.7	19.53 ± 0.08	0°569	2454108.656	486.1	19.47 ± 0.08	0°581
2454099.898	632.8	19.59 ± 0.08	0°569	2454108.723	486.6	19.46 ± 0.09	0°581
2454099.965	632.7	19.52 ± 0.08	0°569	2454108.789	487.5	19.29 ± 0.07	0°581
2454100.032	632.7	19.48 ± 0.08	0°569	2454108.857	487.0	19.48 ± 0.09	0°581
2454100.099	633.3	19.44 ± 0.08	0°569	2454108.924	487.1	19.31 ± 0.08	0°581
2454100.166	632.6	19.52 ± 0.08	0°570	2454108.991	487.0	19.25 ± 0.07	0°581
2454100.233	632.7	19.41 ± 0.07	0°570	2454109.058	486.6	19.44 ± 0.08	0°581
2454100.300	632.7	19.51 ± 0.08	0°570	2454109.124	487.6	19.39 ± 0.08	0°581
2454100.366	632.1	19.45 ± 0.07	0°570	2454109.192	487.0	19.48 ± 0.09	0°581
2454100.434	632.0	19.52 ± 0.08	0°570	2454109.258	487.0	19.61 ± 0.09	0°581
2454100.768	634.6	19.41 ± 0.07	0°571	2454109.521	1089.7	19.50 ± 0.07	0°581
2454100.835	634.5	19.76 ± 0.09	0°571	2454109.590	1355.8	19.52 ± 0.06	0°581
2454100.902	693.0	19.75 ± 0.09	0°571	2454109.660	1571.7	19.44 ± 0.05	0°581
2454100.969	634.6	19.74 ± 0.10	0°571	2454109.728	1748.0	19.45 ± 0.05	0°581
2454101.036	693.0	19.56 ± 0.08	0°571	2454109.795	1749.5	19.46 ± 0.05	0°581
2454101.103	634.5	19.55 ± 0.08	0°571	2454109.853	617.8	19.60 ± 0.10	0°581
2454101.170	634.5	19.38 ± 0.07	0°572	2454109.921	671.8	19.39 ± 0.08	0°581

Table 1 (continued)

Julian date	Exp. time (s)	B magnitude	Phase angle
2454109.988	553.6	19.50 ± 0.09	0°581
2454110.063	1749.6	19.45 ± 0.05	0°581
2454110.129	1750.0	19.47 ± 0.05	0°581
2454110.197	1749.4	19.52 ± 0.05	0°581
2454110.263	1749.3	19.47 ± 0.05	0°581
2454110.321	488.2	19.43 ± 0.10	0°581
2454110.344	384.0	19.32 ± 0.09	0°581
2454110.388	665.2	19.53 ± 0.10	0°581
2454110.457	901.4	19.52 ± 0.08	0°581
2454110.526	1043.6	19.35 ± 0.06	0°581
2454110.595	1515.9	19.54 ± 0.06	0°581
2454110.663	1575.4	19.61 ± 0.06	0°581
2454110.730	1575.7	19.57 ± 0.06	0°581
2454110.796	1575.9	19.36 ± 0.05	0°581
2454111.598	1452.3	19.53 ± 0.06	0°581
2454111.666	1452.3	19.42 ± 0.06	0°582
2454111.732	1452.4	19.43 ± 0.05	0°582
2454111.799	1451.9	19.52 ± 0.06	0°582
2454111.867	1363.2	19.53 ± 0.06	0°582
2454111.934	1364.2	19.52 ± 0.06	0°582
2454112.001	1364.1	19.45 ± 0.06	0°582
2454112.068	1364.2	19.40 ± 0.06	0°582
2454112.131	753.5	19.41 ± 0.07	0°582
2454112.397	546.4	19.50 ± 0.10	0°582
2454112.465	841.1	19.45 ± 0.08	0°582
2454112.530	389.5	19.26 ± 0.10	0°582
2454112.597	449.0	19.37 ± 0.10	0°581
2454112.671	980.2	19.39 ± 0.06	0°581
2454112.735	980.2	19.58 ± 0.07	0°581
2454112.802	929.6	19.51 ± 0.07	0°581
2454112.870	921.2	19.62 ± 0.08	0°581
2454112.936	921.4	19.54 ± 0.07	0°581
2454113.004	921.2	19.44 ± 0.07	0°581
2454113.070	920.8	19.45 ± 0.07	0°581
2454113.137	921.3	19.35 ± 0.06	0°581
2454113.206	597.1	19.47 ± 0.08	0°581
2454113.287	613.2	19.51 ± 0.08	0°581
2454113.401	512.4	19.49 ± 0.10	0°581
2454113.470	808.0	19.50 ± 0.08	0°581
2454113.681	1438.5	19.51 ± 0.06	0°581
2454113.756	611.5	19.42 ± 0.08	0°581
2454113.809	1599.0	19.58 ± 0.06	0°581
2454113.876	1599.1	19.56 ± 0.06	0°581
2454113.943	1598.8	19.41 ± 0.05	0°581
2454114.010	1598.5	19.57 ± 0.06	0°581
2454114.077	1598.0	19.49 ± 0.05	0°581
2454114.140	1008.6	19.73 ± 0.09	0°581
2454114.679	1639.6	19.45 ± 0.05	0°581
2454114.746	1577.3	19.49 ± 0.05	0°581
2454114.813	1576.9	19.54 ± 0.06	0°581
2454114.880	1577.4	19.65 ± 0.06	0°581
2454114.947	1577.3	19.58 ± 0.06	0°581
2454115.014	1577.3	19.51 ± 0.05	0°581
2454115.081	1576.9	19.41 ± 0.05	0°581
2454115.141	565.6	19.60 ± 0.11	0°581
2454115.683	1629.4	19.52 ± 0.05	0°580
2454115.750	1630.0	19.52 ± 0.06	0°580
2454115.818	1629.1	19.55 ± 0.06	0°580
2454115.884	1591.1	19.56 ± 0.06	0°580
2454115.951	1591.9	19.53 ± 0.06	0°580
2454116.018	1595.2	19.53 ± 0.06	0°580
2454116.085	1595.0	19.57 ± 0.06	0°580
2454116.154	560.4	19.50 ± 0.08	0°580
2454116.688	1594.7	19.59 ± 0.06	0°580
2454116.755	1594.2	19.55 ± 0.06	0°580
2454116.822	1594.2	19.57 ± 0.06	0°580
2454116.889	1594.0	19.52 ± 0.05	0°580
2454116.955	1594.6	19.45 ± 0.05	0°580
2454117.023	1593.2	19.48 ± 0.05	0°580
2454117.089	1594.6	19.56 ± 0.06	0°579

half-maximum (FWHM) of Eris and the 26 comparison stars was 2''/3. We found the aperture radius for optimum signal-to-noise ratio to be close enough to the 3''/0 aperture radius recommended by Li et al. (2006) that we adopted a 3''/0 aperture radius through-

out. We determined the magnitude correction for each frame using the ensemble photometry algorithm of Honeycutt (1992). With the photometric stability of UVOT these corrections are small, but non-negligible.

The Sun–Eris–Earth distance varied over the time period of observations and the reported measurements have been scaled to remove this known effect (<1% over the time period). The Sun–Eris–Earth phase angle also varied over the time period of observations between 0°535 and 0°582 (see Table 1). The phase coefficient for Eris in the B-band is zero within uncertainty ($-0.004 \pm 0.028 \text{ mag deg}^{-1}$; Rabinowitz et al., 2007), implying $\leq 0.0015 \text{ mag}$ of variation in the Swift data due to phase angle variation. Any brightness variation due to phase angle is well below our detection limits, and we have not attempted to scale the data to remove the phase angle effect.

The measured count rate of photons from Eris is low, approximately $0.6 \text{ photons s}^{-1}$, and the estimated uncertainty in any individual measurement is large, ranging between 0.05 and 0.13 mag with a median and mean of 0.08 mag. This spread of uncertainty per measurement is almost entirely explained by variable exposure times, necessitated by telescope and instrument scheduling issues. The resulting measurements of Eris are given in Table 1 and shown in Fig. 1. Also shown in Fig. 1 are the mean daily measured magnitudes of Eris. Weighting the individual measurements by their estimated uncertainties we find a mean B magnitude of Eris of 19.494 ± 0.007 , where the final uncertainty is estimated from the standard deviation of the measurements divided by $\sqrt{220}$.

Throughout the observations Eris moved across the background field of stars and galaxies and one possible explanation for any observed variability would be the blending of background objects into the aperture used to measure the flux of Eris. Fig. 2 is a combined image of the entire dataset with the positions of Eris during our observations overplotted. To test for possible background source contamination we performed aperture photometry, using the same technique as above, for each position on the combined image where we had observed Eris. The standard deviation of this photometry was $0.0004 \text{ photons s}^{-1}$ with a maximum excursion from the mean of $0.0006 \text{ photons s}^{-1}$. Given a mean count rate of $\sim 0.6 \text{ photons s}^{-1}$ for Eris, the maximum background source contribution to any observed variation in brightness on Eris is 0.001 mag. This is much smaller than the measured photometric uncertainties and demonstrates that background stars and galaxies did not significantly contaminate the measured Eris fluxes. Dysnomia, the known moon of Eris, is far too faint to have influenced our measurements.

3. Discussion

The Lomb–Scargle periodogram (Press et al., 1992) for these data is shown in Fig. 3A. The significance levels are calculated following the technique suggested by Press et al. (1992), which is to shuffle the data, randomly reassigning observed magnitudes to observation times, and recalculate the periodogram. This operation is performed repeatedly and the peak power in each shuffled periodogram is recorded. The significance levels are determined from $1 - f$, where f is the fraction of the samples for which the highest peak is greater than the power level in question. Two peaks (at ~ 1.1 and ~ 15 days) are at suggestive levels of significance. The data are shown phased to these periods in Figs. 3B and 3C.

Periodograms are powerful tools, but have serious limitations. These data and the ~ 15 day peak are a case study in some of the hazards of periodograms if incorrectly interpreted. One should be extremely wary of strong peaks at periods longer than $\sim 1/3$ – $1/2$ of the total time period covered. The phased data of Fig. 3B show significant gaps in data coverage, which is an additional warning sign in periodogram analysis that results may not be trustworthy.

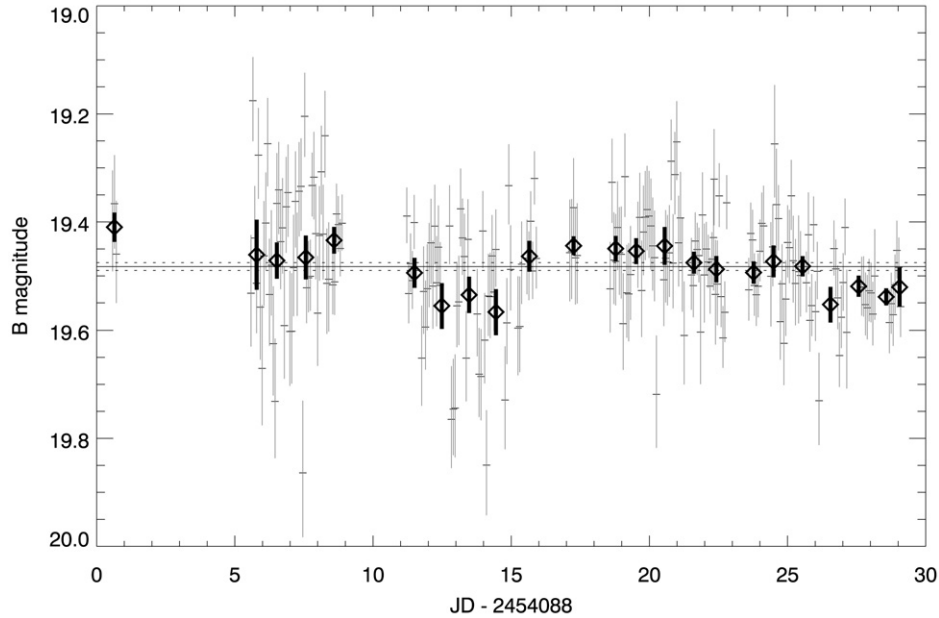


Fig. 1. Each of the 220 *Swift* measurements of Eris in the *B* filter is shown along with its estimated photometric uncertainty. Overplotted as diamonds are the daily means of the data with uncertainties estimated from the standard deviation within each day. Also shown is the mean magnitude of the entire dataset, with 1σ estimated uncertainty.

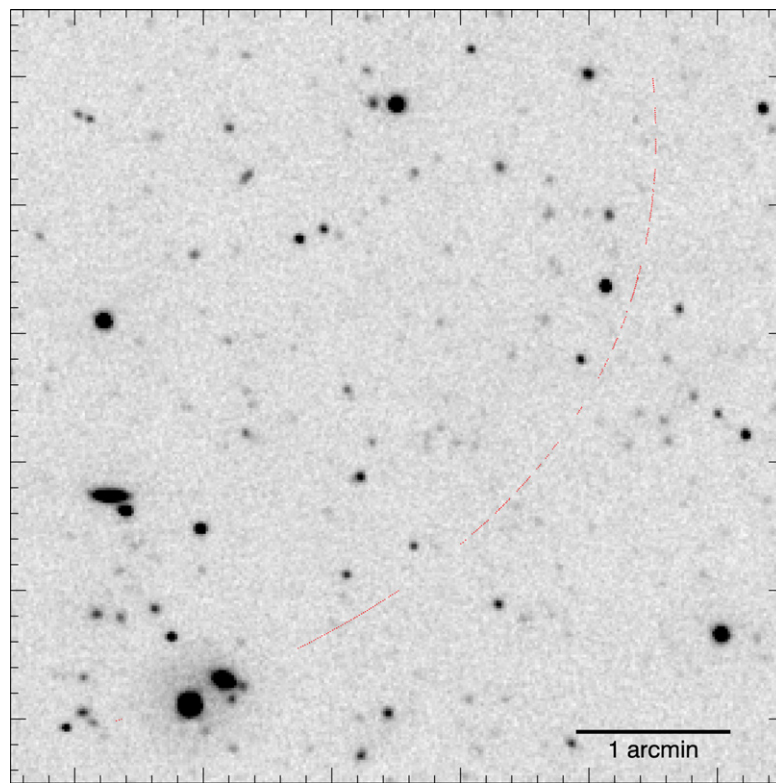


Fig. 2. Combination of all *Swift* *B* images. The gray scale of the image is scaled linearly between $\pm 0.3\%$ of the mean flux of Eris. Overplotted is the position of Eris at the time of each exposure used in the analysis.

From Fig. 3A it would be very tempting to conclude that we detected a ~ 15 day period in Eris, but the data incompletely span only approximately twice this length of time. Examination of the statistics of the variability of the daily mean does not support the detection of a 15 day period. Although the human eye is drawn to the three consecutive daily mean magnitudes in Fig. 1 that lie $>1\sigma$ fainter than the overall mean of the dataset (JD 2454100–2454102), these appear to be a statistical fluke. A simple Monte Carlo simulation reveals that in a Gaussian noise dataset of 23

points (the number of daily means in Fig. 1) about 36% of the time there will be three consecutive data points that all sit $1-3\sigma$ above the mean or all sit $1-3\sigma$ below the mean. Due to these issues we strongly discount the significance of the peak at ~ 15 days.

More interesting is the peak at ~ 1.1 days, which has a significance level of 97%. There are no obvious issues in the phased data of Fig. 3C. To probe the validity of this possible ~ 1.1 day period we ran a variety of tests on our data. We split the dataset in

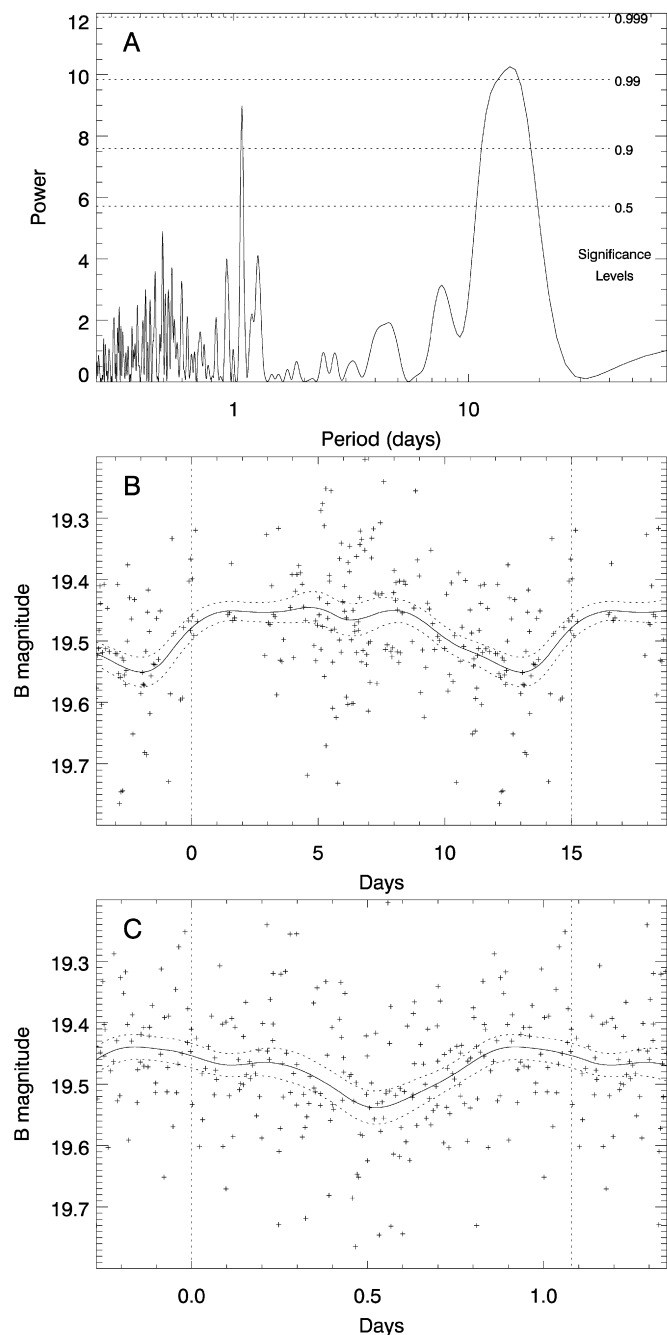


Fig. 3. (A) Periodogram of *Swift* data calculated using the FASPER algorithm of Press et al. (1992). The significance levels are calculated via a Monte Carlo approach as suggested in Press et al. (1992). (B) *Swift* measurements of Eris phased to a period of 15.0 days. Continuously overplotted is a running mean of the nearest 20 phased data points, along with the 1σ estimated uncertainty in that mean. (C) *Swift* measurements of Eris phased to a period of 1.08 days. Continuously overplotted is a running mean of the nearest 20 phased data points, along with the 1σ estimated uncertainty in that mean. We strongly discount the calculated significance level of the 15 day period as our dataset covered only 28 days.

half and found a similar result from each half, although with the expected lower confidence level due to fewer data. We ran a sequence of tests in which we randomly selected half of the data points to analyze and again found similar results. We searched the data for any possible correlations, e.g. flux of Eris with position on the detector, but identified none that could explain the signal seen in Fig. 3C or that could not be ruled out by examination of the ensemble of comparison stars. We examined the Lomb–Scargle pe-

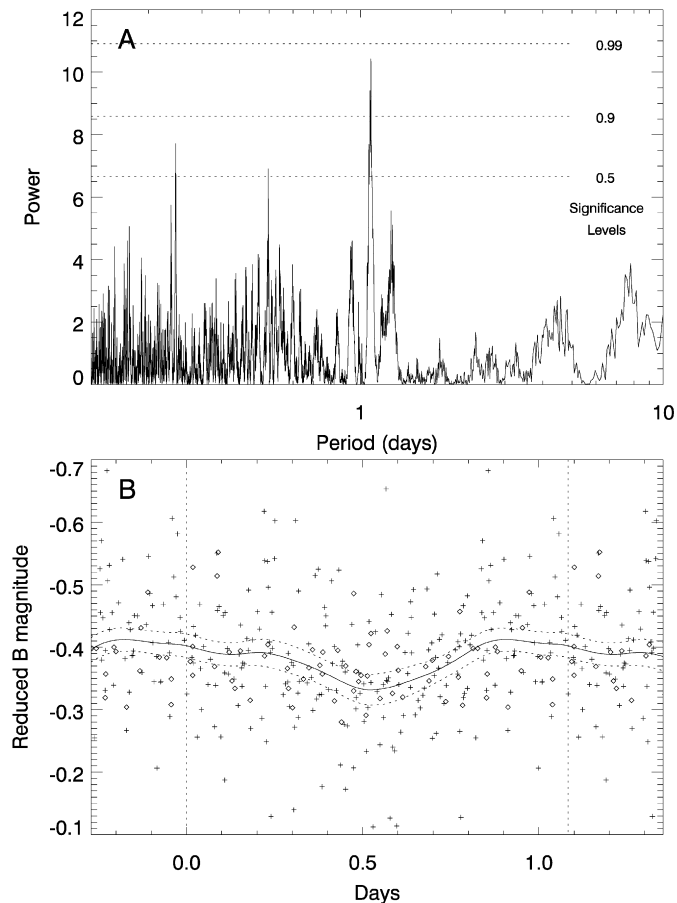


Fig. 4. (A) Periodogram of the combined *Swift* and Rabinowitz et al. (2007) dataset calculated using the FASPER algorithm of Press et al. (1992). The significance levels are calculated via a Monte Carlo approach as suggested in Press et al. (1992). (B) Combined dataset phased to a period of 1.08 days. *Swift* data are shown as plus signs (+), while the Rabinowitz et al. (2007) data are shown as diamonds (\diamond). Continuously overplotted is a running mean of the nearest 20 phased data points, along with the 1σ estimated uncertainty in that mean. The addition of the Rabinowitz et al. (2007) data slightly improve the statistical significance of the recovered periodicity.

riodogram for each of the 26 comparison stars. As expected, given that we had eliminated potential comparison stars with obvious periodicities, none of the 26 comparison stars displayed peaks in the periodogram above a significance level of 90%.

To further test the validity of the possible ~ 1.1 day period we combined the *Swift* dataset with the *B*-band measurements of Rabinowitz et al. (2007), which is the one other published dataset with a significant number of high-quality *B*-band measurements. After scaling the *Swift* measurements to the reduced magnitude system of Rabinowitz et al. (2007) the periodogram of the combined dataset is shown in Fig. 4A. The peak of the periodogram remains at approximately the same period (1.08 days) as with the *Swift* dataset alone, although the significance level of the peak increases slightly to nearly 99%. The combined data phased to this 1.08 day period are shown in Fig. 4B. The results from the combined dataset look very similar to the results from the *Swift* dataset alone.

We can find no reason to discount the validity of the ~ 1.1 day period. Using the 50% confidence levels of the periodogram as a guide for estimating the uncertainty in the period, we report that Eris appears to be rotating once every 1.08 ± 0.02 days with a peak-to-valley amplitude of nearly 0.1 mag. At the modest level of confidence available from these data the periodic signal appears less like a sinusoid and more like what would be expected from

a large dark patch on the partially hidden hemisphere of an otherwise homogeneous body. At rotational phases where the patch is hidden from the observer the light curve is constant. A dip in the light curve is observed during the rotational phases that the dark patch is visible to the observer. Additional observations will be required to confirm this result and more precisely determine the rotation period of Eris.

Of the previously published datasets the long-term sequence of Rabinowitz et al. (2007) and the several nights of precision photometry of Sheppard (2007) are the most likely to have been able to identify the apparent periodicity seen in these *Swift* data.

Sheppard (2007) did precision *R*-band photometry of Eris over several hours on each of three contiguous nights in October 2005 and three contiguous nights in December 2005. A careful evaluation of the approximately daily sampling of their data reveals that a periodic signal such as that suggested by the *Swift* data in Fig. 3C could have been missed. The signal in Fig. 3C appears nearly constant over ~50% of the rotation period, while phased to a period of 1.08 days the Sheppard (2007) data cover less than half of this rotation period.

The magnitude of variation in the light curve of Eris is likely a function of wavelength. Most of the surface of Eris must be uniformly bright to achieve the high *V*-band geometric albedo ($86 \pm 7\%$; Brown et al., 2006). Any darker patches are likely to be photochemically processed hydrocarbons, which will have a red color. At longer wavelengths (e.g. *R*-band and *I*-band) the albedo of these red patches will be closer to the albedo of the uniformly bright dominant surface material. At shorter wavelengths (e.g. the *B*-band used here by *Swift*) there will be greater contrast between these red patches and the rest of the surface of Eris. This is directly analogous to what is seen on Pluto, where the light curve at *B*-band has an amplitude of ~0.1 mag greater than the amplitude at *R*-band (Buratti et al., 2003). Thus, the light curve of Eris is likely to be less pronounced at longer wavelengths (e.g. *R*-band) than the shorter wavelength *B*-band observed with *Swift*.

Rabinowitz et al. (2007) reported observations in several filters, taken once per night over many months. The analysis of the Rabinowitz et al. (2007) data is thus dependent upon the simultaneous fitting of color terms and phase function coefficients. We experimented with inserting fake signals into the Rabinowitz et al. (2007) data with a range of periods and amplitudes consistent with the periodicity detected in the *Swift* data. We then used the same analysis tools as before to search for periodicity. In many cases the inserted periodicity is recovered, however whether the fake signal is detected and the period at which it is detected is strongly dependent on the exact amplitude and period of the fake signal. This is primarily because the test periods (~1.08 days) are near the sampling interval (~1 day) of the Rabinowitz et al. (2007) data. In some example cases varying the inserted signal's period by only 0.005 days made the difference between a strong detection and a non-detection. However, as described above, the combination of the *B*-band measurements of Rabinowitz et al. (2007) with the *Swift* measurements reported here improves the significance of the retrieved periodicity somewhat from that of the *Swift* data alone.

A coherent picture of Eris is emerging. The surface is primarily covered in bright methane frost, much like the brightest patches

of Pluto's surface. However, our results suggest that the surface of Eris is not perfectly homogeneous. Under thermal equilibrium the vapor pressure of methane on Eris is negligible at its current near-perihelion distance of 97.5 AU. If the entire surface of Eris is uniformly covered in very high albedo methane frost, even at aphelion (38.2 AU) the equilibrium surface temperature of Eris is not warm enough to generate significant methane evaporation from the surface. This presents a problem as methane frost in the outer Solar System is expected to redden and darken due to photochemical processing, but Eris appears bright and shows no sign of redness. This suggests the methane frost deposits on its surface must be fresh and a replenishment mechanism is required. Our detection of variability is consistent with regional darker areas on the surface. At aphelion the widespread high albedo regions will not warm enough to sublimate methane into the atmosphere, however the small darker areas will be heated by the increased insolation to kickoff feedback effects that lead to dramatic global surface change, generating a temporary atmosphere and replenishing the methane surface each Eris year.

Acknowledgments

We thank David Rabinowitz and an anonymous referee.

References

- Brown, M.E., Schaller, E.L., 2007. The mass of dwarf planet Eris. *Science* 316, 1585.
- Brown, M.E., Schaller, E.L., Roe, H.G., Rabinowitz, D.L., Trujillo, C.A., 2006. Direct measurement of the size of 2003 UB313 from the Hubble Space Telescope. *Astrophys. J.* 643, L61–L63.
- Brown, M.E., Trujillo, C.A., Rabinowitz, D.L., 2005. Discovery of a planetary-sized object in the scattered Kuiper belt. *Astrophys. J.* 635, L97–L100.
- Buie, M.W., Tholen, D.J., Wasserman, L.H., 1997. Separate lightcurves of Pluto and Charon. *Icarus* 125, 233–244.
- Buratti, B.J., Hillier, J.K., Heinze, A., Hicks, M.D., Tryka, K.A., Mosher, J.A., Ward, J., Garske, M., Young, J., Atienza-Rosel, J., 2003. Photometry of Pluto in the last decade and before: Evidence for volatile transport? *Icarus* 162, 171–182.
- Carraro, G., Maris, M., Bertin, D., Parisi, M.G., 2006. Time series photometry of the dwarf planet ERIS (2003 UB313). *Astron. Astrophys.* 460, L39–L42.
- Cruikshank, D.P., Roush, T.L., Moore, J.M., Sykes, M., Owen, T.C., Bartholomew, M.J., Brown, R.H., Tryka, K.A., 1997. The Surfaces of Pluto and Charon. In: *Pluto and Charon*. University of Arizona Press, Tucson, pp. 221–267.
- Duffard, R., Ortiz, J.L., Santos Sanz, P., Mora, A., Gutiérrez, P.J., Morales, N., Guirado, D., 2008. A study of photometric variations on the dwarf planet (136199) Eris. *Astron. Astrophys.* 479, 877–881.
- Honeycutt, R.K., 1992. CCD ensemble photometry on an inhomogeneous set of exposures. *Publ. Astron. Soc. Pacific* 104, 435–440.
- Li, W., Jha, S., Filippenko, A.V., Bloom, J.S., Pooley, D., Foley, R.J., Perley, D.A., 2006. The calibration of the *Swift* UVOT optical observations: A recipe for photometry. *Publ. Astron. Soc. Pacific* 118, 37–61.
- Lin, H.-W., Wu, Y.-L., Ip, W.-H., 2007. Observations of dwarf planet (136199) Eris and other large TNOs on Lulin observatory. *Adv. Space Res.* 40, 238–243.
- Press, W.H., Teukolsky, S.A., Vetterling, W.T., Flannery, B.P., 1992. *Numerical Recipes in FORTRAN: The Art of Scientific Computing*, second ed. Cambridge University Press, Cambridge.
- Rabinowitz, D.L., Schaefer, B.E., Tourtellotte, S.W., 2007. The diverse solar phase curves of distant icy bodies. I. Photometric observations of 18 trans-neptunian objects, 7 Centaurs, and Nereid. *Astron. J.* 133, 26–43.
- Sheppard, S.S., 2007. Light curves of dwarf plutonian planets and other large Kuiper belt objects: Their rotations, phase functions, and absolute magnitudes. *Astron. J.* 134, 787–798.
- Stern, S.A., Buie, M.W., Trafton, L.M., 1997. HST high-resolution images and maps of Pluto. *Astron. J.* 113, 827–885.